

Assessment of the cosmic distance duality relation using Gaussian Process

Purba Mukherjee¹^{*} and Ankan Mukherjee^{2,3}[†]

¹Department of Physical Sciences, Indian Institute of Science Education and Research Kolkata, Mohanpur 741246, India

²Department of Physics, Bangabasi College, Kolkata 700009, India

³Centre for Theoretical Physics, Jamia Millia Islamia, New Delhi 110025, India.

Accepted ??, Received ??; in original form ??

ABSTRACT

Two types of distance measurement are important in cosmological observations, the angular diameter distance d_A and the luminosity distance d_L . In the present work, we carried out an assessment of the theoretical relation between these two distance measurements, namely the cosmic distance duality relation, from type Ia supernovae (SN-Ia) data, the Cosmic Chronometer (CC) Hubble parameter data, and baryon acoustic oscillation (BAO) data using Gaussian Process. The luminosity distance curve and the angular diameter distance curve are extracted from the SN-Ia data and the combination of BAO and CC data respectively using the Gaussian Process. The distance duality relation is checked by a non-parametric reconstruction using the reconstructed H , d_L , and the volume-averaged distance D_V . We compare the results obtained for different choices of the covariance function employed in the Gaussian Process. It is observed that the theoretical distance duality relation is in well agreement with the present analysis in 2σ for the overlapping redshift domain $0 \leq z \leq 2$ of the reconstruction.

Key words: cosmology – distance duality – distance scale (luminosity distance, angular diameter distance) – Gaussian process

1 INTRODUCTION

Distance measurement in cosmology gives an idea about the mutual separation between two objects or events in the universe on radial null trajectories which terminate at the observer. It serves as one of the most crucial and important tasks involved in cosmography, helping us to establish a standard relation between the observational data with theoretical models, thus setting up the rudimentary framework. Distance measures are often used to tie some observable quantity (such as the luminosity of a distant star, or angular size of the acoustic peaks in the Cosmic Microwave Background power spectrum) to some other quantity that is not directly observable, but is more convenient for calculations.

Cosmologists use different definitions of *distance* from the observer to a celestial object at redshift z , of which two are extremely useful. They are the luminosity distance d_L , and the angular diameter distance d_A respectively. The former is defined by the relation between bolometric flux and bolometric luminosity, which can further be connected to the absolute magnitude M and apparent magnitude m of an astronomical object. Likewise, the latter one is a distance associated with an object's physical size, and its angular size, projected on the celestial sphere. They are connected through

the cosmic distance-duality relation (CDDR) (Etherington 1933, 2007) given as,

$$d_L = d_A(1+z)^2. \quad (1)$$

The CDDR was first proved by Etherington in the context of a Friedmann-Lemaître-Robertson-Walker (FLRW) metric, and is often recognized as Etherington's reciprocity theorem.

The reciprocity theorem is considered to be correct for any general metric theories of gravity in any background based on two fundamental hypotheses. Firstly, when number of photons is conserved during cosmic evolution (Ellis 1971, 2007), and secondly, when gravity is described by a metric theory with photons travelling on unique null geodesics in a Riemannian geometry. The coupling of photons with unknown particles (Bassett & Kunz 2004a), the extinction of photons by intergalactic dust (Corasaniti 2006), the variation of fundamental constants (Ellis et al. 2013) can lead towards a violation of CDDR. As cosmography is strongly dependent on the validity of CDDR, a little deviation from it may indicate the possibility of some exotic physics beyond the standard model or the presence of systematic errors in observations (Bassett & Kunz 2004a,b). Therefore, with the increasing quality and quantity of observational data, evaluating the reliability of CDDR has received much attention lately.

^{*} E-mail: pm14ip011@iiserkol.ac.in

[†] Email: ankan.ju@gmail.com

The CDDR can straight away be put to test utilizing the

luminosity distance $d_L(z)$ and the angular diameter distance $d_A(z)$ measurements at the same redshift z . The distance measures can generally be obtained through observations of the type Ia supernovae (SN-Ia), high redshift galaxies (HII), angular diameter of galaxy clusters, galaxy cluster gas mass fraction, strong gravitational lensing (SGL), cosmic microwave background (CMB), gamma ray bursts (GRB), radio compact sources, baryon acoustic oscillations (BAO), Gravitational Waves (GWs), and so on. The type-Ia supernovae data (Suzuki et al. 2012; Betoule et al. 2014; Scolnic et al. 2018) generally serve as major sources for estimating d_L with high precision. Nevertheless, determining the angular diameter distance d_A is neither simple nor effortless as that of d_L . The combined data of the X-ray and Sunyaev-Zeldovich (SZ) effect of galaxy clusters (Filippis et al. 2005; Bonamente et al. 2006), the baryon acoustic oscillations (BAO) in the galaxy power spectrum (Beutler et al. 2011; Blake et al. 2012; Anderson et al. 2014; Kazin et al. 2014), the angular size of ultra-compact radio sources based on the approximately consistent linear size (Kellermann 1993; Gurvits 1994; Gurvits, Kellermann & Frey 1999; Jackson 2004), the images of quasars that are strongly gravitational lensed by foreground galaxies (Cao et al. 2015; Liao et al. 2016) are amongst a few feasible measurement practices. However, computing d_A as discussed above have their respective merit and limitations. Li & Lin (2018); Lin, Li & Li (2018) provides us with a brief discussion in this context.

While testing for validity of CDDR, the prime difficulty experienced is that both d_L and d_A are not computed at the same redshift z . Several approaches have been proposed to resolve this drawback. These involves the nearest neighbourhood method (Holanda, Lima & Ribeiro 2010; Liao et al. 2016), the interpolation method (Liang et al. 2013), and the Gaussian Processes (Nair, Jhingan & Jain 2015; Rana et al. 2017; Li & Lin 2018) method. It deserves mention that only data points in the overlapping redshift range are available for CDDR verification. Until now, no evidence for CDDR violation has been recorded from the reconstruction techniques. In the nearest neighbour approach Holanda, Lima & Ribeiro (2010) considered two sub-samples of SN-Ia from the Constitution data along with two samples of galaxy clusters compiled by Filippis et al. and Bonamente et al. by combining the SZ effect and X-ray surface brightness. The SN-Ia redshifts of each sub-sample by were carefully chosen within a redshift separation $\Delta z < 0.005$, so that they coincide with those of the associated galaxy cluster samples, thereby allowing a direct test for the CDDR. However, this approach suffers from several inconsistencies, viz. significant reduction of statistical information encoded in the data sets as pointed out by Max-Moerbeck et al. (2018). This redshift-matching problem from the nearest neighbour method was overcome by Cardone et al. (2012), applying a local regression technique to the SN-Ia d_L data at the concerned redshift windows with adjustable bandwidth. But again, this idea could not be easily generalized to strongly correlated data, thus rejecting a majority of data points, thereby leading to incorrect estimation. Ma, Corasaniti & Bassett (2016); Ma & Corasaniti (2018) addressed this issue by using Bayesian statistical techniques, precisely a Monte Carlo method, which compresses correlated luminosity distance data at specific points in log-redshift.

Reconstruction of the CCCR has previously been often addressed in literature. They are categorized into the cosmological model-dependent tests (Uzan, Aghanim & Mellier 2004; Avgoustidis et al. 2010; Holanda, Lima & Ribeiro 2011; Lima, Cunha &

Zanchin 2011; Nair, Jhingan & Jain 2011; Jhingan, Jain & Nair 2014; Holanda, Busti & Alcaniz 2016; Hu & Wang 2018), and the cosmological model-independent analysis (Holanda, Lima & Ribeiro 2010; Li, Wu & Yu 2011; Gonçalves, Holanda & Alcaniz 2011; Nair, Jhingan & Jain 2012; Meng et al. 2012; Chen, Zhou & Fu 2015; Holanda & Barros 2016; Liao et al. 2016; Rana et al. 2016; Holanda, Pereira & da Costa 2017; Holanda et al. 2019; Xu & Huang 2020; Zheng et al. 2020). Nair, Jhingan & Jain (2011) studied the validity of six different parametrized CDDR using the Union2 SN data. Holanda, Gonçalves & Alcaniz (2012) used the gas mass fraction measurements of galaxy clusters from SZ effect and X-ray surface brightness observations. Gonçalves et al. (2015) considered the gas mass fraction measurements reported by the Atacama Cosmology Telescope (ACT) survey along with Union2.1 SN-Ia compilation. da Costa, Busti & Holanda (2015) used galaxy clusters and Hubble data measurements. Holanda & Barros (2016) utilized the nearest neighbour approach considering SGL and JLA SN-Ia weighted average data. Liao et al. (2016) considered a compilation of SGL and JLA SN-Ia, along with galaxy cluster samples and FRIB radio galaxies. Rana et al. (2016) worked with the JLA SN-Ia data, and samples from radio galaxies. Hu & Wang (2018) tested CDDR in the $R_h = ct$ Universe using the regression method. Li & Lin (2018) used the ultra-compact radio sources in combination with Union 2.1 SN-Ia data. Ma & Corasaniti (2018) used the BAO data from BOSS DR12 and WiggleZ survey, along with JLA SN-Ia compilation. Ruan, Melia & Zhang (2018) considered SGL and HII galaxy Hubble diagram to obtain constraints on the CDDR parametrizations. Testing CDDR from Future GWs Sirens was done by Fu, Zhou & Chen (2019). However, all these works involve a functional form for the CDDR chosen at the outset, followed by an estimation of parameters. This is undoubtedly biased, as a specific parametric form for the CDDR is already chosen.

In the present work, the Supernova distance modulus data, Cosmic Chronometer measurements of the observational Hubble data and the Baryon Acoustic Oscillation data have been utilized in examining the validity of CDDR in a non-parametric way. The reconstruction is performed adopting the model-independent Gaussian Processes (GP) method. For a detailed overview one can refer to the Gaussian Process website¹. A non-parametric reconstruction of CDDR using the GP method is barely addressed in the existing literature. Nair, Jhingan & Jain (2015) compared distance measurements from the Union2 sample of supernovae with BAO data from SDSS, 6dFGS and the latest BOSS and WiggleZ surveys. Rana et al. (2017) presented a new way to constrain the CDDR using different dynamic and geometric properties of SGL along with JLA SN-Ia observations. Results showed no violation of CDDR. Here, we use the recent Pantheon sample of SN-Ia for obtaining d_L , and d_A are derived considering the volume-averaged BAO compilation data in combination with the CC $H(z)$ data, at the same domain of redshift. We attempt to perform this reconstruction avoiding any fiducial bias on the cosmological parameters included in the data sets.

This paper is arranged as follows. Section 2 contains the details on the reconstruction method. In section 3, the observational data used in the present work have been briefly reviewed. The results

¹ <http://www.gaussianprocess.org>

obtained are presented in section 4. We conclude the manuscript in section 5 with an overall discussion about the results.

2 RECONSTRUCTION METHODOLOGY

In this section we shall discuss the details of the reconstruction technique and define the necessary physical quantities involved in our work. It is already mentioned that an entirely non-parametric, model-independent approach is utilized in the present study. A reconstruction of the cosmic distance duality relation has been carried out directly from the observational data without assuming any specific parametrization, or an *a priori* fiducial background cosmology. We utilize the Gaussian Process method as our numerical tool in this work.

To test the validity of the cosmic distance duality relation, we analyse the following redshift dependence of CDDR, given by,

$$\eta(z) = \frac{d_L}{d_A(1+z)^2}. \quad (2)$$

In case of $\eta = 1$ we recover back equation (1), which implies a non-violation of the standard CDDR. Any deviation of η from unity ($\eta \neq 1$) indicates a non-validation of CDDR. In order to test the CDDR directly from observations, we perform a model independent GP reconstruction of η using the publicly available GaPP² (Gaussian Processes in Python) code developed by Seikel, Clarkson & Smith (2012).

The uncertainty associated with the reconstructed function η can be calculated by the standard error propagation formula,

$$\sigma_\eta = \eta \sqrt{\left(\frac{\sigma_{d_L}}{d_L}\right)^2 + \left(\frac{\sigma_{d_A}}{d_A}\right)^2}, \quad (3)$$

The Gaussian Process is a generalization of the Gaussian probability distribution. It generalizes the idea of a Gaussian distribution characterized by discrete data points to the continuous limit. Assuming the observational data, say D , obeys a Gaussian distribution with mean and variance, the posterior distribution of the target function $F = F(z_i)_{i=1}^n$ describing the data $\{(z_i, D_i) | i = 1, \dots, n\}$ can be expressed via the joint Gaussian distribution of $D(z_i)$'s. Thus, given a set of Gaussian-distributed data points one can use GP to reconstruct the target function, and also obtain the associated confidence levels, without assuming a concrete parametrization of the target function. For this the key element is a covariance function $k(z, \tilde{z})$ which correlates values of the reconstructed function D at redshift points z and \tilde{z} separated by $|z - \tilde{z}|$ distance units. This covariance function $k(z, \tilde{z})$ depends on a set of hyperparameters (i.e., the characteristic length scale l and the signal variance σ_f). l describes the distance one needs to move roughly in input space before the function value changes significantly, whereas σ_f determines a distinct change in the function value. Different choices for the covariance function may have different effects on the reconstruction. Here, we take into account the Squared Exponential as well as three orders of the Matérn covariance functions in performing our analysis. The Squared Exponential covariance function is defined as,

$$k(z, \tilde{z}) = \sigma_f^2 \exp\left(-\frac{(z - \tilde{z})^2}{2l^2}\right) \quad (4)$$

and the Matérn covariance is given by,

$$k_{\nu=p+\frac{1}{2}}(z, \tilde{z}) = \sigma_f^2 \exp\left(\frac{-\sqrt{2p+1}}{l}|z - \tilde{z}|\right) \times \frac{p!}{(2p)!} \sum_{i=0}^p \frac{(p+i)!}{i!(p-i)!} \left(\frac{2\sqrt{2p+1}}{l}|z - \tilde{z}|\right)^{p-i}. \quad (5)$$

In cases for the Matérn covariance function, the orders of the polynomials are taken as ($p = 2, 3, 4$), consequently the parameter ν has the values $(\frac{5}{2}, \frac{7}{2}, \frac{9}{2})$.

In order to implement the Gaussian Process and reconstruct the function F , one needs to know the hyperparameters σ_f and l . They can be trained by maximizing the marginal likelihood, which is a marginalization over function values $\{F(z_i)\}$ at observational redshift locations $\{z_i\}_{i=1}^n$. Note that this marginal likelihood is independent of the redshift points where we want to reconstruct the function. For a Gaussian prior the log marginal likelihood is given by,

$$\ln \mathcal{L} = -\frac{1}{2}(\mathbf{D} - \boldsymbol{\mu})^T [K(\mathbf{Z}, \mathbf{Z}) + \mathbf{C}]^{-1} (\mathbf{D} - \boldsymbol{\mu}) + \frac{1}{2} \ln |K(\mathbf{Z}, \mathbf{Z}) + \mathbf{C}| - \frac{n}{2} \ln 2\pi \quad (6)$$

where, $\boldsymbol{\mu} = \{\mu(z_i)\}_{i=1}^n$ is the mean function and $K(\mathbf{Z}, \mathbf{Z})$ is the covariance matrix given by $[K(\mathbf{Z}, \mathbf{Z})]_{ij} = k(z_i, z_j)$ at $\mathbf{Z} = \{z_i\}_{i=1}^n$ observational redshift points. \mathbf{C} is the covariance matrix of the data and n is the dimension of \mathbf{D} or \mathbf{Z} .

3 OBSERVATIONAL DATASETS

It is already mentioned that the SN-Ia distance modulus data, the Cosmic Chronometer measurements of the Hubble parameter and the BAO volume-averaged distance data are adopted in the present context. In the following section, these data sets and the way they are utilized in the present analysis are discussed.

3.1 $d_L(z)$ from SN-Ia data

The type Ia supernovae are widely accepted as *standard candles* to measure cosmological distance for their approximately consistent absolute luminosity (Riess et al. 1998; Perlmutter et al. 1999). For the supernova data, we use the recent Pantheon compilation sample by Scolnic et al. (2018) consisting of 1048 SN-Ia data points. The numerical data of the full Pantheon SN-Ia catalogue is publicly available^{3,4}.

The Pantheon compilation is at present the largest sample which consists of different supernovae surveys, including SDSS, SNLS, various LOW- z samples and some HIGH- z samples from HST. We include the covariance matrix along with systematic errors in our calculation. The distance modulus of each supernova is given by,

$$\mu(z) = 5 \log_{10} \left(\frac{d_L(z)}{\text{Mpc}} \right) + 25 \quad (7)$$

² <https://github.com/carlosandrepaes/GaPP>

³ <http://dx.doi.org/10.17909/T95Q4X>

⁴ <https://archive.stsci.edu/prepds/ps1cosmo/index.html>

Table 1. Table showing the reconstructed value of H_0 (in units of $\text{km Mpc}^{-1} \text{s}^{-1}$) for different choices of the covariance function, from the CC data.

$k(z, \bar{z})$	Matérn 9/2	Matérn 7/2	Matérn 5/2	Squared Exponential
H_0	68.471 ± 5.081	68.684 ± 5.204	68.858 ± 5.466	67.356 ± 4.765

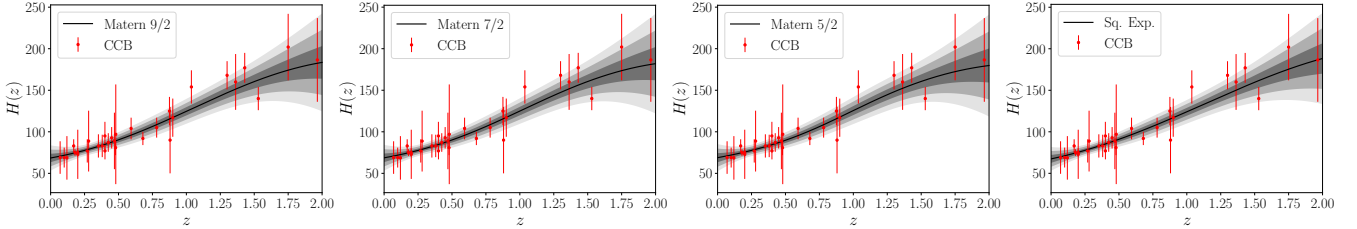

Figure 1. Plots for $H(z)$ (in units of $\text{km Mpc}^{-1} \text{s}^{-1}$) reconstructed from CC data using the Matérn 9/2, Matérn 7/2, Matérn 5/2 and Squared Exponential covariance function (from left to right) respectively. The solid black line is the best fitting curve and the associated 1σ , 2σ and 3σ confidence regions are shown in lighter shades.

Table 2. Table showing the marginalized constraints on M_B , Ω_{m0} and r_d (in units of Mpc) for different choices of the covariance function using equations (20), (22) and (24) respectively.

$k(z, \bar{z})$	Matérn 9/2	Matérn 7/2	Matérn 5/2	Squared Exponential
M_B	-19.388 ± 0.006	-19.387 ± 0.006	-19.387 ± 0.006	-19.391 ± 0.006
Ω_{m0}	0.305 ± 0.004	0.302 ± 0.004	0.299 ± 0.005	0.321 ± 0.004
r_d	146.116 ± 0.336	146.086 ± 0.340	146.044 ± 0.350	146.193 ± 0.326

where d_L is the luminosity distance. So,

$$d_L(z) = 10 \left(\frac{z}{5} - 5 \right) \quad (8)$$

in units of Mpc.

Now, the distance modulus of SN-Ia can be derived from the observation of light curves through the empirical relation,

$$\mu_{\text{SN}} = m_B^* + \alpha X_1 - \beta C - M_B + \Delta_M + \Delta_B \quad (9)$$

where X_1 and C are the stretch and colour parameters, and M_B is the absolute magnitude in the B-band for SN-Ia. α and β are two nuisance parameters, Δ_M is a distance correction based on the host-galaxy mass of the SN-Ia and Δ_B is a distance correction based on predicted biases from simulations. Usually, the nuisance parameters α and β are optimized simultaneously with the cosmological model parameters or are marginalized over. However, this method is model dependent. In the Pantheon sample, the corrected apparent magnitude $m_B = m_B^* + \alpha X_1 - \beta C$ along with Δ_M and Δ_B corrections are reported following the BEAMS with Bias Corrections [BBC] (Kessler & Scolnic 2017) framework. Therefore, the colour, stretch corrections are no longer required, so we can fix $\alpha = \beta = 0$ and proceed with $\mu_{\text{SN}} = (m_B - M_B)$.

The statistical uncertainty \mathbf{C}_{stat} and systematic uncertainty \mathbf{C}_{sys} are also available. So, the total uncertainty matrix of distance modulus is,

$$\Sigma_{\mu} = \mathbf{C}_{\text{stat}} + \mathbf{C}_{\text{sys}} \quad (10)$$

The uncertainty of $d_L(z)$ is propagated from the uncertainties of μ using the standard error propagation formula,

$$\Sigma_{d_L} = \mathbf{D}_1 \Sigma_{\mu} \mathbf{D}_1^T \quad (11)$$

where the superscript ‘T’ denotes the transpose of a matrix. Also, \mathbf{D}_1 is a Jacobian matrix given by

$$\mathbf{D}_1 = \text{diag} \left(\frac{\ln 10}{5} \mathbf{d}_L \right), \quad (12)$$

where \mathbf{d}_L is a vector whose components are the luminosity distances of all SN-Ia.

We know the absolute magnitude of SN-Ia is degenerate with the Hubble parameter, so we obtain the marginalized constraints on M_B following a similar procedure as in Mukherjee & Banerjee (2021).

3.2 $D_V(z)$ from BAO data

The baryon acoustic oscillations are regular, periodic fluctuations in the visible baryonic matter density, and are widely used as ‘‘standard rulers’’ to measure the distances in cosmology. Here we use data points from the following surveys:

- (i) 6dFGS (Beutler et al. 2011) at effective redshift $z = 0.106$.
- (ii) WiggleZ Dark Energy Survey (Blake et al. 2012) at effective redshifts $z = 0.44, 0.6$ and 0.73 .
- (iii) MGS and SDSS (LOWZ and CMASS samples) (Xu et al. 2013; Anderson et al. 2014; Ross et al. 2015; Gil-Marín et al. 2015) at effective redshift $z = 0.15, 0.32, 0.57$.
- (iv) BOSS DR12 (Alam et al. 2017) at $z = 0.38, 0.51, 0.61$.
- (v) eBOSS DR14 LRG (Bautista et al. 2018) and quasar (Ata et al. 2018) sample at redshifts $z = 0.72, 1.52$ respectively.
- (vi) HIGHZ Lyman- α measurement in BOSS DR12 (Bautista et al. 2017) at redshift $z = 2.33$.

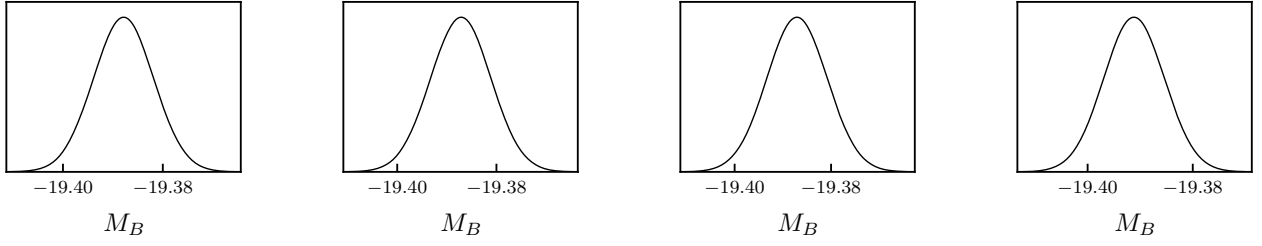


Figure 2. Plots for marginalized likelihood of absolute magnitude M_B using the Matérn 9/2, Matérn 7/2, Matérn 5/2 and Squared Exponential covariance function (from left to right) respectively.

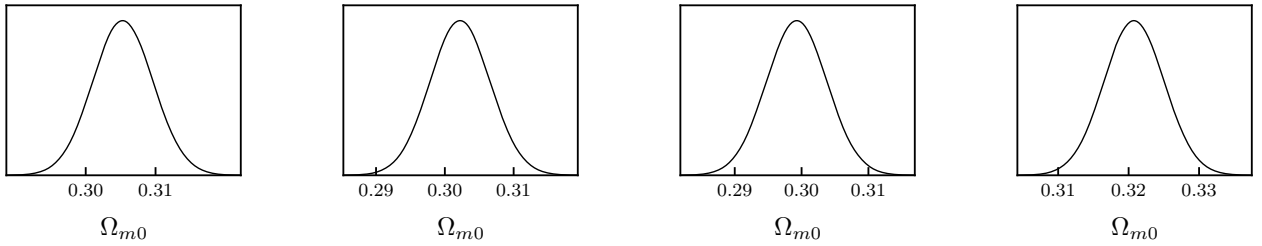


Figure 3. Plots for marginalized likelihood of matter density parameter Ω_{m0} using the Matérn 9/2, Matérn 7/2, Matérn 5/2 and Squared Exponential covariance function (from left to right) respectively.

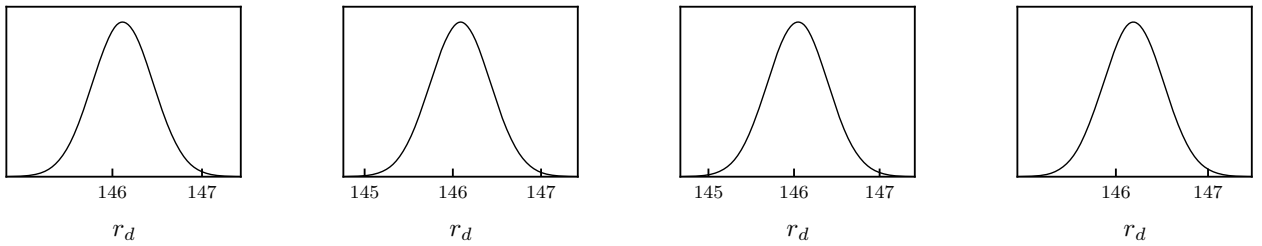


Figure 4. Plots for marginalized likelihood of comoving sound horizon at drag epoch r_d (in units of Mpc) using the Matérn 9/2, Matérn 7/2, Matérn 5/2 and Squared Exponential covariance function (from left to right) respectively.

(vii) Correlations of Ly α absorption in eBOSS DR14 at $z = 2.34$ (de Sainte Agathe et al. 2019).

(viii) Cross-correlation of Ly α absorption and quasars in eBOSS DR14 at $z = 2.35$ (Blomqvist et al. 2019).

For the purpose of our analysis, we shall use the volume-averaged D_V distance data. The WiggleZ DES data is cosmological parameter dependent (Ω_{m0} and H_0), hence the uncertainties associated is propagated in the evaluation of the distance errors, that are used for the GP evaluation. We define,

$$D_V(z) = \left[(1+z)^2 d_A^2(z) \frac{cz}{H(z)} \right]^{\frac{1}{3}}, \quad (13)$$

therefore

$$d_A(z) = \left[\frac{D_V^3(z) H(z)}{c z (1+z)^2} \right]^{\frac{1}{2}} \quad (14)$$

and $r_{d, \text{fid}} = 147.49$ is considered unless explicitly specified in the datasets. The comoving sound horizon at the drag epoch r_d is de-

fined as (Eisenstein & Hu 1998),

$$r_d = \int_{z_d}^{\infty} \frac{c_s(z)}{H(z)} dz \quad (15)$$

with $c_s(z)$ the sound speed and z_d the redshift at the drag epoch. Equation (15) can be approximated as,

$$r_d \approx \frac{44.5 \log \left(\frac{9.83}{\Omega_{m0} h_0^2} \right)}{\sqrt{1 + 10 (\Omega_{b0} h_0^2)^{3/4}}} \quad (16)$$

for the standard model cosmology where we rewrite, $h_0 = \frac{H_0}{100}$ in a dimensionless way. In this particular work, constraints on the comoving sound horizon at the drag epoch r_d (in Mpc) has been obtained keeping it a free parameter in our analysis.

3.3 $H(z)$ from CC data

The Hubble parameter $H(z)$ can be directly obtained from the differential redshift time derivative, by calculating the spectroscopic

Table 3. Table showing the value of r_d (in units of Mpc) for different choices of the covariance function, considering the approximated definition from equation (16).

$k(z, \bar{z})$	Matérn 9/2	Matérn 7/2	Matérn 5/2	Squared Exponential
r_d	149.828 ± 12.059	149.959 ± 12.313	150.134 ± 12.921	149.181 ± 11.496

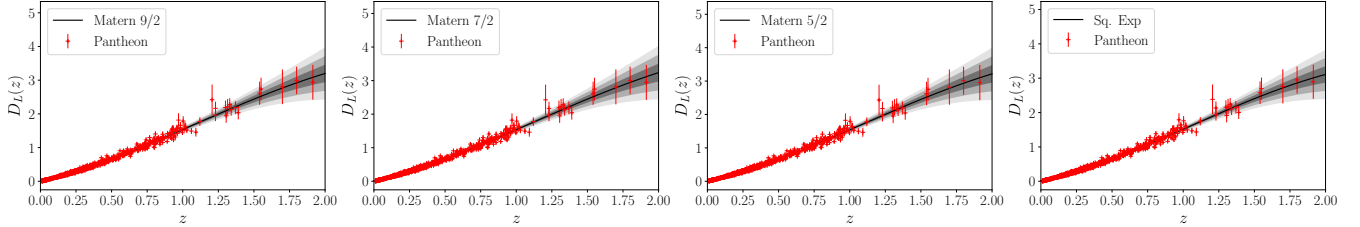


Figure 5. Plots for the reconstructed dimensionless or normalized luminosity distance D_L considering the Matérn 9/2, Matérn 7/2, Matérn 5/2 and Squared Exponential (from left to right) covariance function. The black solid lines represent the best fitting curves. The associated 1σ , 2σ and 3σ confidence levels are shown by the shaded regions.

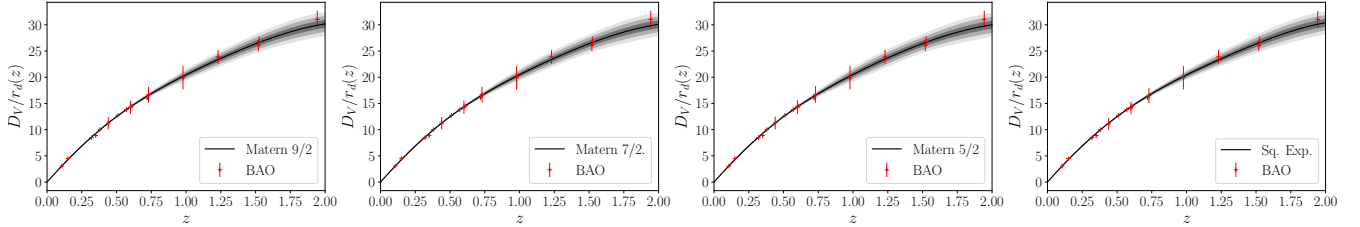


Figure 6. Plots for the reconstructed dimensionless ratio of volume-averaged distance to the comoving sound horizon at drag epoch $\frac{D_V}{r_d}$ considering the Matérn 9/2, Matérn 7/2, Matérn 5/2 and Squared Exponential (from left to right) covariance function. The black solid lines represent the best fitting curves. The associated 1σ , 2σ and 3σ confidence levels are shown by the shaded regions.

differential ages of passively evolving galaxies, usually called the Cosmic Chronometer (CC) method. In this work we use the 32 CCH data points measured by considering the BC03 stellar population synthesis model (Simon et al. 2005; Stern et al. 2010; Moresco et al. 2012; Zhang et al. 2014; Moresco 2015; Moresco et al. 2016; Ratsimbazafy et al. 2017), covering the redshift range up to $z \sim 2$. These measurements do not assume on any particular cosmological model.

4 RESULTS

We reconstruct the Hubble parameter $H(z)$ using the GP method and the results are shown Fig. 1. The value of the Hubble constant H_0 obtained from this model independent reconstruction is shown in Table 1. Again, we normalize the reconstructed $H(z)$ data to obtain the dimensionless or reduced Hubble parameter $E(z) = H(z)/H_0$. We calculate the uncertainty in $E(z)$ by the standard technique of error propagation as,

$$\sigma_E^2 = \frac{\sigma_H^2}{H_0^2} + \frac{H^2}{H_0^4} \sigma_{H_0}^2, \quad (17)$$

where σ_{H_0} is the error associated with H_0 .

Utilizing the reconstructed $E(z)$ function, the normalised comoving distance D for a flat spacetime is evaluated numerically

using the trapezoidal integration rule such that,

$$D(z) = \int_0^z \frac{dz'}{E(z')}. \quad (18)$$

The error associated with D , σ_D is obtained by following a similar integration of the function $E(z)$ including its 1σ error uncertainties.

We perform another GP reconstruction on the apparent magnitudes m_B of the SN-Ia data and reconstruct them at the same redshift z as that of the CC data. On substituting equation (18) in equation (7), we estimate the reconstructed distance modulus from the Hubble data as, $\mu_H = 5 \log_{10} [D(1+z)] + 25$ along with its 1σ error uncertainty σ_{μ_H} given by,

$$\sigma_{\mu_H} = \frac{5}{\ln 10} \frac{\sigma_D}{D}. \quad (19)$$

The absolute magnitude of SN-Ia is degenerate with the Hubble parameter H_0 . We get the marginalized constraints on M_B by minimizing the χ^2 function,

$$\chi_{\text{SN}}^2 = \sum \Delta\mu^T \cdot \Sigma^{-1} \cdot \Delta\mu, \quad (20)$$

considering a uniform prior $M_B \in [-35, -5]$, where $\Delta\mu = (\mu_{\text{SN}} - \mu_H)$ and $\Sigma = \Sigma_{\mu_{\text{SN}}} + \sigma_{\mu_H}^2$ respectively.

Further we perform the reconstruction of $\frac{D_V}{r_d}$ from the BAO data compilation in the same redshift range $0 < z < 2$. The WiggleZ DES data measures the acoustic scale parameter $A(z)$ given

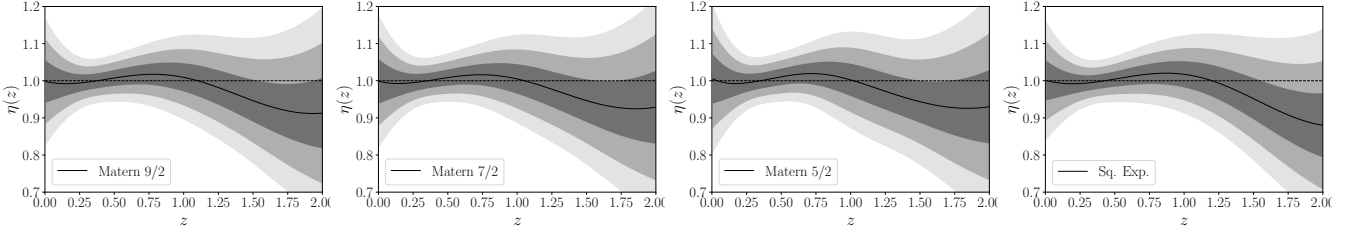


Figure 7. Plots for the reconstructed cosmic distance duality ratio η considering the Matérn 9/2, Matérn 7/2, Matérn 5/2 and Squared Exponential (from left to right) covariance function using r_d from Table 2. The black solid lines represent the best fitting curves. The associated 1σ , 2σ and 3σ confidence levels are shown by the shaded regions.

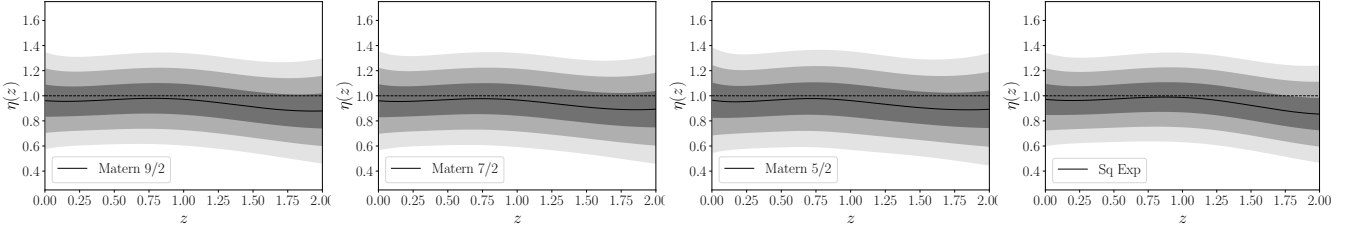


Figure 8. Plots for the reconstructed cosmic distance duality ratio η considering the Matérn 9/2, Matérn 7/2, Matérn 5/2 and Squared Exponential (from left to right) covariance function using r_d from Table 3. The black solid lines represent the best fitting curves. The associated 1σ , 2σ and 3σ confidence levels are shown by the shaded regions.

by,

$$A(z) = D_V \frac{\sqrt{\Omega_{m0} H_0^2}}{cz} \quad (21)$$

As the matter density parameter Ω_{m0} is correlated with H_0 we constrain Ω_{m0} assuming a fiducial Λ CDM model,

$$\chi_H^2 = \sum_i \frac{\left[E(z_i) - \sqrt{\Omega_{m0}(1+z_i)^3 + 1 - \Omega_{m0}} \right]^2}{\sigma_E^2(z_i)} \quad (22)$$

with uniform prior $\Omega_{m0} \in [0.01, 0.7]$ using the reconstructed $E(z)$ data, for the same H_0 obtained in Table 1. For the remaining BAO data sets we reconstruct D_V/r_d by dividing with $r_{d, \text{fid}} = 147.49$ wherever applicable. We can rewrite (13) in terms of the reconstructed $D(z)$ and $H(z)$ from the CC data as,

$$D_V|_H = \left[\frac{c^2 D^2(z)}{H_0^2} \frac{cz}{H(z)} \right]^{\frac{1}{3}} = \frac{c}{H_0} \left[\frac{D^2(z)z}{E(z)} \right]^{\frac{1}{3}} \quad (23)$$

Finally we minimize the χ^2 function,

$$\chi_{\text{BAO}}^2 = \sum \frac{\left(\frac{D_V}{r_d} \Big|_{\text{BAO}} - \frac{D_V}{r_d} \Big|_H \right)^2}{\sigma_{\frac{D_V}{r_d}}^2 \Big|_{\text{BAO}} + \sigma_{\frac{D_V}{r_d}}^2 \Big|_H} \quad (24)$$

and obtain the marginalized constraints on r_d for a uniform prior assumption $r_d \in [130, 160]$.

Uncertainty in the parameters M_B , Ω_{m0} and r_d are obtained by a Markov Chain Monte Carlo (MCMC) analysis. Here, we adopt a python implementation of the ensemble sampler for MCMC, the emcee⁵, introduced by Foreman-Mackey et al. (2013). Finally, we

plot the results using the GetDist⁶ module of python, developed by Lewis (2019). Plots for the marginalized M_B , Ω_{m0} and r_d constraints are shown in the Figures 2, 3 and 4. The best fitting values are given in Table 2.

Another method for estimating the value of r_d is from equation (16). Using the marginalized constraints of Ω_{m0} , and the reconstructed value of H_0 we evaluate r_d along with its 1σ uncertainty by propagation of error. Moreover, we assumed the value $\Omega_{b0} h_0^2 = 0.022383$ from Planck 2018 Aghanim et al. (2020). Result for the calculated values of r_d using the aforementioned procedure is shown in Table 3.

Thereafter, we plot the reconstructed dimensionless functions $D_L(z)$ [where $D_L = \frac{H_0 d_L}{c}$ is the normalized luminosity distance] and $\frac{D_V}{r_d}(z)$ in the redshift range $0 < z < 2$ as that of reconstructed $H(z)$, using Gaussian Process (GP) for different choices of the covariance function in Fig 5 and 6 respectively. The specific points (in the H , D_L and $\frac{D_V}{r_d}$ plots) with error bars represent the observational data used in reconstruction. The hyperparameters (σ_f, l) are optimized by maximizing log marginal likelihood while performing the GP.

Finally, we perform the non-parametric reconstruction of η directly using the reconstructed $H(z)$, $d_L(z)$ and $D_V(z)$ following the relation,

$$\eta(z) = \frac{d_L \sqrt{cz}}{D_V^{\frac{3}{2}} H^{\frac{1}{2}} (1+z)}. \quad (25)$$

Plots for the reconstructed $\eta(z)$ are shown in Fig 7 and 8 considering different choices of the covariance function. In case of Fig 7, we

⁵ <https://github.com/dfm/emcee>

⁶ <https://github.com/cmbant/getdist>

make use the marginalized constraints on r_d obtained via equation (24). Fig 8 is plot considering the approximated value of r_d derived from equation (16). It appears so in Fig 8, that the uncertainty does not increase significantly at higher redshift, as compared to Fig 7. However, comparing the Y-axes range of both the plots, it can be clearly seen that Fig 7 is better constrained than that of 8. This could be the effect of 1σ uncertainty in r_d which quite large in case of Fig 8 as compared to Fig 7, tabulated in Tables 3 and 2 respectively. The black solid line represents the best fit values of η . The shaded regions correspond to the 68 percent (1σ), 95 percent (2σ) and 99.7 percent (3σ) confidence levels (CL). Plots reveal that the reconstructed values of $\eta(z)$ in the low redshift range $0 < z < 1$ remains very close to unity. At higher redshift $z > 1.5$, in case of the Matérn 5/2 and 7/2 covariance functions, CDDR is always allowed in 1σ for Fig 8 and barely in case of Fig 7. Again, considering the Matérn 9/2 and Squared Exponential covariance functions, CDDR is almost allowed within the 1σ uncertainty in Fig 8 with increasing redshift $z > 1.5$. Nonetheless, CDDR is always allowed within a 2σ uncertainty, which indicate a non-violation of CDDR in the late time universe for all cases studied.

5 DISCUSSION

In the present study, viability of the cosmic distance duality relation is investigated by a non-parametric model-independent method. The distance modulus measurements of type Ia supernovae from the latest Pantheon sample, the cosmic chronometer measurements of the Hubble parameter, and the recent measurements of volume-averaged Baryon Acoustic Oscillation data are utilized in the analysis. Firstly, we perform a reconstruction of the luminosity distance d_L from the Pantheon SN-Ia compilation. A reconstruction of the Hubble parameter $H(z)$ from the CC data, followed by another reconstruction of D_V from the BAO has been carried out next using Gaussian Process. The analysis has been performed in the same domain of redshift for four choices of the covariance function, namely the Squared exponential, Matérn 9/2, Matérn 7/2 and Matérn 5/2 covariance. The angular distance d_A are obtained via combining the reconstructed H and D_V from the CC and BAO data respectively.

Finally, the reconstructed functions viz. luminosity distance $d_L(z)$, Hubble parameter $H(z)$ and the volume-averaged distance D_V have been combined to get the cosmic distance-duality ratio $\eta(z)$. The reconstructed η curve is obtained directly from the data without assuming any prior functional form as ansatz. A common feature is that the best-fit curve for η , shown in Fig 7 and 8, is close to $\eta = 1$ curve in the range $0 < z < 1$, and $\eta = 1$ is always included in 1σ for the redshift range $0 < z < 1.5$. However with increasing z , i.e., $z > 1.5$, in case of the Matérn 5/2 and 7/2 covariance functions, $\eta = 1$ is mostly included in 1σ for Fig 8 and barely in 1σ for Fig 7. In Fig 8, $\eta = 1$ value almost remains within the 1σ uncertainty for the Matérn 9/2 and Squared Exponential covariance functions. But, $\eta = 1$ is always included in 2σ for all choices of the covariance functions, in case of both Fig 7 and 8. It has already been mentioned that, this contrast in results arises due to the 1σ uncertainty difference in r_d values considered, while performing the reconstruction. As the BAO data points are mostly concentrated up to $z \approx 1$, the reconstructed η is well constrained up to $z \approx 1$. The uncertainty in the $\eta(z)$ curves increase with increasing redshift.

It deserves mention that we obtained the marginalized

constraints on M_B by keeping the nuisance parameters α , β , colour, stretch and bias corrections fixed using the BBC framework, for the Pantheon compilation of SN-Ia. Fixing the value of M_B from the global Λ CDM fits from Scolnic et al. (2018), may result in inconsistencies as M_B is degenerate with H_0 . In case of the BAO $\frac{D_V}{r_d}$ data, the comoving sound horizon at photon drag epoch, r_d is constrained considering a fiducial measure on $r_{d, \text{fid}}$ equal to 147.49 wherever applicable. Again BAO measurement from WiggleZ in Blake et al. (2012), are cosmological parameter dependent, precisely H_0 and Ω_{m0} . Therefore we have also derived the constraints on Ω_{m0} assuming a fiducial Λ CDM model. The uncertainties on these parameters are propagated properly for the evaluation of error in the distance measurements. As there may be correlations between these parameters H_0 , M_B , Ω_{m0} and r_d keeping these values fixed may have a serious effect on the model-independent nature of reconstruction, if proper care is not taken.

The Gaussian process method has previously been used for a non-parametric reconstruction of η in literature. Nair, Jhingan & Jain (2015) utilized Union 2.1 SN-Ia data compilation, BAO data of SDSS, 6dF Galaxy Survey, WiggleZ and BOSS ($z = 0.57$), and observational Hubble data compilation to reconstruct the luminosity distance, the angle-averaged distance and the Hubble rate, using the GP regression technique in the redshift range $0.1 < z < 0.73$. Our work is similar to the work by Nair, Jhingan & Jain, where the SN-Ia and BAO data were particularly used. But there are quite a few differences to list. We have used the latest updated Pantheon SN-Ia compilation which spans a redshift range $z = 2.26$, instead of the Union 2.1 sample with available data points limited up to $z = 1.41$. Here, constraints have been obtained on a wider range of overlapping redshift $0 < z < 2$, and tighter constraints are obtained in the low redshift regime due to availability of more number of BAO data points. Another non-parametric reconstruction of the cosmic distance-duality relation by Rana et al. (2017) using different dynamic and geometric properties of SGLs along with JLA SN-Ia observations, do not favour any deviation of CDDR and are in concordance with the standard value of unity within a 2σ confidence region. In this case, the sole difference lies in terms of the data sets involved, and the redshift range considered for reconstruction. As for Rana et al. the reconstruction was mainly focused on the redshift range of $0 < z < 1$. Zhou & Li (2019) reconstructed the distance-redshift relation from observations of the Dark Energy Survey SN-Ia with simulated fiducial $H(z)$ data, and obtained that, except for the very low redshift range $z < 0.2$, there is no obvious deviation from the theoretical CDDR. The prime objective of work by Zhou & Li was to test the fidelity of Gaussian processes for cosmography where CDDR was reconstructed as a consistency check. The present work shows that the GP successfully reproduces the CDDR even at higher redshift.

The results obtained in the present analysis are totally in agreement with those from the existing literature, discussed above. We have extended the analysis to higher redshift. But due to the lack of observational data points at higher redshift, the uncertainty increases. We can conclude that all the recent studies of cosmic distance measurements support the theoretical CDDR at low redshift ($z < 1.5$). Future higher redshift observations of BAO, SN-Ia and other observables would be able to provide tighter constraints on CDDR at higher redshift. Similar analysis with future observations would be useful to decide whether theoretically CDDR is equally

valid at high redshift, or redshift dependent higher order correction terms are essentially required.

ACKNOWLEDGEMENT

The authors would like to thank Prof. Narayan Banerjee for useful discussions and suggestions. The authors would also like to acknowledge the anonymous referee for the important comments and constructive suggestions that led to a substantial improvement of the paper. AM acknowledges the financial support from the Science and Engineering Research Board (SERB), Department of Science and Technology, Government of India as a National Post-Doctoral Fellow (NPDF, File no. PDF/2018/001859).

DATA AVAILABILITY

Authors can confirm that all relevant source data are included in the article. The datasets generated during and/or analysed during the current study are available from the corresponding author on reasonable request.

REFERENCES

- Aghanim N. et al. [Planck Collaboration], 2020, *A&A*, 641, A6.
- Alam S., Ata M., Bailey S., Beutler F. et al., 2017, *MNRAS*, 470, 2617.
- Alcaniz J. S. et al., 2017, *Fundam. Theor. Phys.*, 187, 11.
- Anderson L. et al., 2014, *MNRAS*, 441, 24.
- Ata, M., Baumgarten, F., Bautista, J. et al. 2018, *MNRAS*, 473, 4773.
- Avgoustidis A., Burrage C., Redondo J., Verde L., & Jimenez R., 2010, *J. Cosmology Astropart. Phys.*, 10, 024.
- Bassett B. A., Kunz M., 2004, *Phys. Rev. D*, 69, 101305.
- Bassett B. A., Kunz M., 2004, *ApJ*, 607, 661.
- Bautista J. E. et al., 2017, *A&A*, 603, A12.
- Bautista, J. E., Vargas-Magaña, M., Dawson, K. S. et al. 2018, *ApJ*, 863, 110.
- Betoule M. et al. [SDSS Collaboration], 2014, *A&A*, 568, A22.
- Beutler, F., Blake, C., Colless, M. et al. 2011, *MNRAS*, 416, 3017.
- Blake C., Brough S., Colless M. et al., 2012, *MNRAS*, 425, 405.
- Blomqvist M. et al., 2019, *A&A*, 629, A86.
- Bonamente M., Joy M. K., LaRoque S. J., Carlstrom J. E., Reese E. D., Dawson K. S., 2006, *ApJ*, 647, 25.
- Cardone V. F., Spiro S., Hook I., Scaramella, R., 2016, *Phys. Rev. D*, 85, 123510.
- Carvalho G. C. et al., 2016, *Phys. Rev. D*, 93, 023530.
- Carvalho G. C. et al., 2017, preprint, arXiv:1709.00271.
- Cao S., Biesiada M., Gavazzi R., Piórkowska A., Zhu Z.-H., 2015, *ApJ*, 806, 185.
- Chen Z., Zhou B., Fu X., 2015, *Int. J. Theo. Phys.*, 55, 1229.
- Corasaniti P. S., 2006, *MNRAS*, 372, 191.
- de Carvalho E. et al., 2018, *J. Cosmology Astropart. Phys.*, 04, 064.
- de Carvalho E. et al., 2020, *MNRAS*, 492, 4469.
- da Costa S. S., Busti V. C., Holanda R. F., 2015, *J. Cosmology Astropart. Phys.*, 10, 061.
- de Sainte Agathe V. et al., 2019, *A&A*, 629, A85.
- Eisenstein, D. J., Hu, W. 1998, *ApJ*, 496, 605.
- Ellis G. F. R., 1971, *General Relativity and Cosmology*, Enrico Fermi Summer School Course XLVII, ed R. K. Sachs, New York Academic.
- Ellis G. F. R., 2007, *Gen. Rel. Grav.*, 39, 1047.
- Ellis G. F. R., Poltis R., Uzan J. P., Weltman A., 2013, *Phys. Rev. D*, 87, 103530.
- Etherington I. M. H., 1933, *The London, Edinburgh, and Dublin Philosophical Magazine and Journal of Science* 15, 761.
- Etherington I. M. H., 2007, *Gen. Rel. Grav.*, 39, 1055.
- De Filippis E., Sereno M., Bautz M. W., Longo G., 2005, *ApJ*, 625, 108.
- Foreman-Mackey D., Hogg D. W., Lang D., Goodman J., 2013, *Publ. Astron. Soc. Pac.*, 125, 306.
- Fu X., Zhou L., Chen J., 2019, *Phys. Rev. D*, 99, 083523.
- Gil-Marín, H., Percival, W. J., Cuesta, A. J. et al. 2016, *MNRAS*, 460, 4210.
- Gonçalves R. S., Holanda R. F. L., Alcaniz J. S., 2011, *MNRAS*, 420, L43.
- Gonçalves R. S., Alcaniz J. S., Carvalho J. C., Holanda R. F. L., 2015, *Phys. Rev. D*, 91, 027302.
- Gurvits L. I., 1994, *ApJ*, 425, 442.
- Gurvits L. I., Kellermann K. I., Frey S., 1999, *A&A*, 342, 378.
- Holanda R. F. L., Lima J. A. S., Ribeiro M. B., 2010, *ApJ*, 722, L233.
- Holanda R. F. L., Lima J. A. S., Ribeiro M. B., 2011, *A&A*, 528, L14.
- Holanda R., Gonçalves R., Alcaniz J., 2012, *J. Cosmology Astropart. Phys.*, 12, 022.
- Holanda R., Barros K., 2016, *Phys. Rev. D*, 94, 023524.
- Holanda R., Busti V., Alcaniz J., 2016, *J. Cosmology Astropart. Phys.*, 02, 054.
- Holanda R., Pereira S., da Costa S. S., 2017, *Phys. Rev. D*, 95, 084006.
- Holanda R., Colaço L., Pereira S., Silva R., 2019, *J. Cosmology Astropart. Phys.*, 06, 008.
- Hu J., Wang F. Y., 2018, *MNRAS*, 477, 5064.
- Jackson J. C., 2004, *J. Cosmology Astropart. Phys.*, 11, 007.
- Jhingan S., Jain D., Nair R., 2014, *J. Phys. Conf. Ser.* 484, 012035.
- Kazin E. A. et al., 2014, *MNRAS*, 441, 3524.
- Kellermann K. I., 1993, *Nature*, 361, 134.
- Kessler R., Scolnic D., 2017, *ApJ*, 836, 56.
- Lewis A., 2019, preprint, arXiv:1910.13970 [astro-ph.IM].
- Li X., Lin H.-N., 2018, *MNRAS*, 474, 313.
- Li Z., Wu P., Yu H., 2011, *ApJ*, 729, L14.
- Liang N., Li Z., Wu P., Cao S., Liao K., Zhu Z.-H., 2013, *MNRAS*, 436, 1017.
- Liao K., Li Z., Cao S., Biesiada M., Zheng X., Zhu Z.-H., 2016, *ApJ*, 822, 74.
- Lima J. A. S., Cunha J. V., Zanchin V. T., 2011, *ApJ*, 742, L26.
- Lin H.-N., Li M.-H., Li X., 2018, *MNRAS*, 480, 3117.
- Ma C., Corasaniti P. S., Bassett B. A., 2016, *MNRAS*, 463, 1651.
- Ma C., Corasaniti P. S., 2018, *ApJ*, 861, 124.
- Max-Moerbeck W., Richards J. L., Hovatta T., et al., 2014, *MNRAS*, 445, 437.
- Meng X.-L., Zhang T.-J., Zhan H., Wang X., 2012, *ApJ*, 745, 98.
- Moresco M., Cimatti A., Jimenez R., Pozzetti L., 2012, *J. Cosmology Astropart. Phys.*, 08, 006.
- Moresco M., 2015, *MNRAS*, 450, L16.
- Moresco M., Pozzetti L., Cimatti A. et al., 2016, *J. Cosmology Astropart. Phys.*, 05, 014.
- Mukherjee P., Banerjee N., 2021, *Euro. Phys. J. C*, 81, 36.
- Nair R., Jhingan S., Jain D., 2011, *J. Cosmology Astropart. Phys.*, 05, 023.
- Nair R., Jhingan S., Jain D., 2012, *J. Cosmology Astropart. Phys.*, 12, 028.
- Nair R., Jhingan S., Jain D., 2015, *Phys. Rev. B*, 745, 64.
- Perlmutter S. et al., 1998, *ApJ*, 517, 565.
- Rana A., Jain D., Mahajan S., Mukherjee A., Holanda R., 2017, *J. Cosmology Astropart. Phys.*, 07, 010.
- Rana A., Jain D., Mahajan S., Mukherjee A., 2016, *J. Cosmology Astropart. Phys.*, 07, 026.
- Ratsimbazafy A. L., Loubser S. I., Crawford S. M. et al., 2017, *MNRAS*, 467, 3239.
- Riess A. G. et al., 1998, *AJ*, 116, 1009.
- Ross, A. J., Samushia, L., Howlett, C. et al. 2015, *MNRAS*, 449, 835.
- Ruan C.-Z., Melia F., Zhang T.-J., 2018, *ApJ*, 866, 31.
- Samushia L., Reid B. A., White M. et al., 2014, *MNRAS*, 439, 3504.
- Scolnic D. M. et al., 2018, *ApJ*, 859, 101.
- Seikel M., Clarkson C., Smith M., 2012, *J. Cosmology Astropart. Phys.*, 06, 036.
- Simon J., Verde L., Jimenez R., 2005, *Phys. Rev. D*, 71, 123001.
- Stern D., Jimenez R., Verde L., Kamionkowski M., Stanford S. A., 2010, *J. Cosmology Astropart. Phys.*, 02, 008.
- Suzuki N., Rubin D., Lidman C. et al., 2012, *ApJ*, 746, 85.
- Uzan J.-P., Aghanim N., Mellier Y., 2004, *Phys. Rev. D*, 70, 083533.

- Xu X., Cuesta A. J., Padmanabhan N., Eisenstein D. J., McBride C. K., 2013, MNRAS, 431, 2834.
- Xu B., Huang Q., 2020, Euro. Phys. J. Plus, 135, 447.
- Zhang C., Zhang H., Yuan S., Zhang T.-J., Sun Y.-C., 2014, Res. Astron. Astrophys., 14, 1221.
- Zheng J. et al., 2019, MNRAS, 484, 442.
- Zheng X., Liao K., Biesiada M., Cao S., Liu T.-H., Zhu Z.-H., 2020, ApJ, 892, 103.
- Zhou H., Li Z. X., 2019, Chinese Phys. C, 43, 035103.